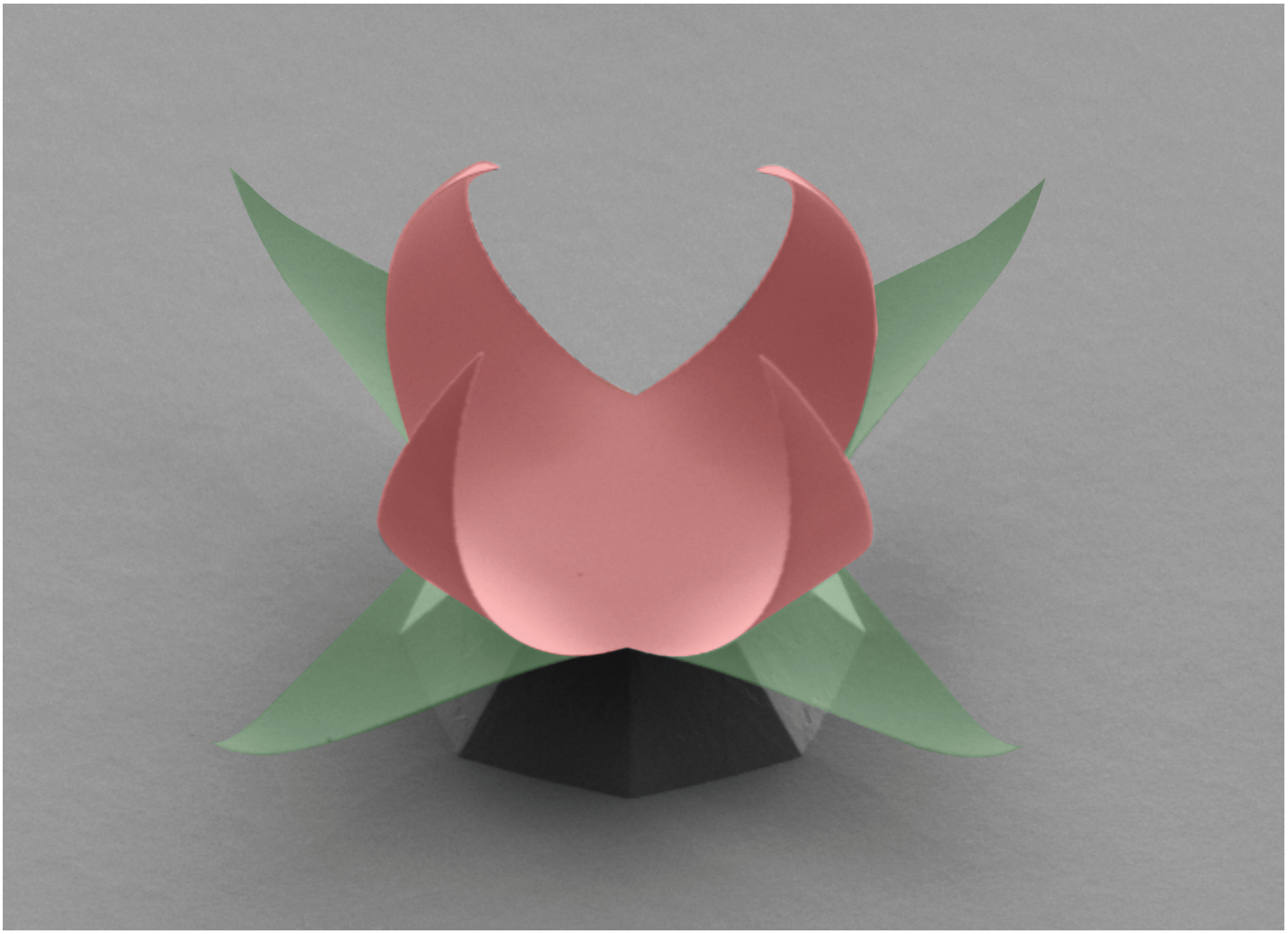

Showcasing research from the Thayer School of Engineering, Dartmouth College, the Department of Mechanical and Automation Engineering, Chinese University of Hong Kong, and the Department of Electrical and Computer Engineering, Michigan State University.

Edge effect of strained bilayer nanofilms for tunable multistability and actuation

Due to misfit strain and the edge stress effect, a Si/Cr (35/10 nm) microclaw can form either an open configuration (in green) or a closed configuration (in red, overlaid together). The global shape of the microclaw can be changed from an open to a closed state and vice versa. Our study showed that the transition from a monostable state to a bistable state occurred when the magnitude of the edge effect increased. The addition of bistability in the nanostructure will significantly expand the scope of its applications in nano-/micro-robotics, energy harvesting, and drug delivery systems.

As featured in:

See L. Zhang, L. X. Dong, Z. Chen *et al.*, *Nanoscale*, 2017, **9**, 2958.

ROYAL SOCIETY OF CHEMISTRY

rsc.li/nanoscale

Registered charity number: 207890

Nanoscale

COMMUNICATION

View Article Online
View Journal | View Issue

Cite this: *Nanoscale*, 2017, **9**, 2958

Received 9th November 2016,
Accepted 21st December 2016

DOI: 10.1039/c6nr08770a

rsc.li/nanoscale

Edge effect of strained bilayer nanofilms for tunable multistability and actuation†

N. Hu,[a] X. Han,[a] S. Huang,[a] H. M. Grover,[a] X. Yu,[a] L. N. Zhang,[a,b] I. Trase,[a] J. X. J. Zhang,[a] L. Zhang,*[c] L. X. Dong*[d] and Z. Chen*[a]

We employed both theoretical and computational models supported by experiments to study the multistable behavior of an edge-effect driven Si/Cr micro-claw. Our study showed that individual micro-claws demonstrate either monostability or bistability as the magnitude of the edge effect is varied.

Three-dimensional (3D) structures have attracted significant attention for their potential application in micro- and nano-electromechanical systems.[1] One prevailing fabrication approach is to scroll a strained, multilayered film by selective etching. A typical bilayer architecture consists of a thin, strained, metallic layer as a stressor and a relatively thick strain-free semiconductor layer,[2] such as Si/SiGe and Si/Cr. The internal strain in the metallic layer initiates the detachment of the bilayer structure from the substrate. In many cases, the bilayer structure can fully recover to its initial configuration.[3] The bilayer structure can be made to roll into a variety of 3D functional structures,[4–7] including ones that can manipulate nano-objects, induce motion, or measure material properties.

Si/Cr strips are commonly fabricated with a thin Cr layer deposited on top of a Si layer by thermal evaporation. Previous experimental studies on Si/Cr strips have confirmed that the scrolling behavior and the diameter of the rolled-up structures can depend on the layer thickness,[8] the strip width,[9,10] the misorientation angle between the strip axis and the preferred scrolling orientation,[11] and anisotropic underetching on different Si substrates.[12] Additional surface and edge effects also play a role in strained microstructures,[13,14] which provides additional freedom when designing 3D geometries.

In this letter, we study how the bistability of a Si/Cr micro-claw (Fig. 1) is influenced due to edge effects through a combined experimental, analytical, and numerical approach. Most studies have focused on bilayer scrolling while overlooking potential multistability in the rolled-up structures. It remains incompletely understood how the multistable behaviors of the Si/Cr nanostructure vary depending on the magnitude of edge effect. This variation may cause the mis-orientation angle. Nanostructures with multiple stable shapes can exhibit more than one stable state and can rapidly switch between those stable states. Such tunable feature can provide additional functionalities when developing nano-elecromechanical/micro-electromechanical systems devices.

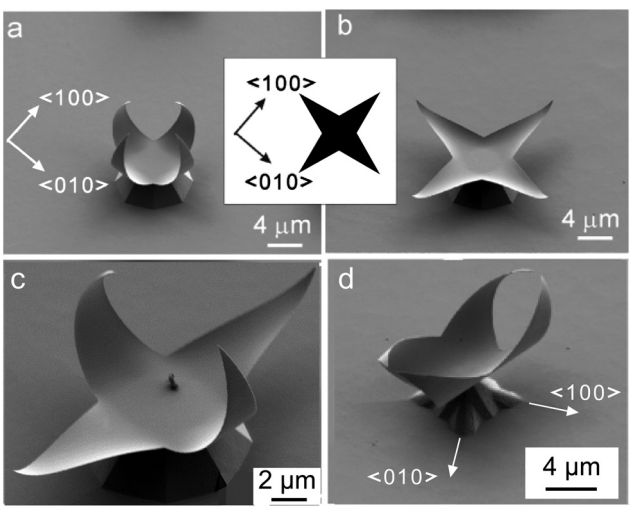

Fig. 1 A field emission scanning electron microscope images of a Si/Cr micro-claw. (a) The closed state. Inset: the initial fabrication pattern. (b) The open state with the same initial pattern as inset. (c) The closed state with each "finger" oriented along a <110> direction. (d) The partially closed state. Si/Cr bilayer films is 45 nm (35/10) thick.

[a]*Thayer School of Engineering, Dartmouth College, Hanover, NH 03755, USA. E-mail: zi.chen@dartmouth.edu*
[b]*Department of Engineering Mechanics, Shanghai Jiao Tong University, Shanghai 200240, China*
[c]*Department of Mechanical and Automation Engineering, Chinese University of Hong Kong, Shatin, N.T. 999077 Hong Kong SAR, China. E-mail: lizhang@mae.cuhk.edu.hk*
[d]*Department of Electrical and Computer Engineering, Michigan State University, East Lansing, MI 48823, USA. E-mail: ldong@egr.msu.edu*

†Electronic supplementary information (ESI) available: Movie of micro-claw closure; nanofabrication and nanorobotic manipulation; table-top experiments; theoretical derivation and notation; finite element modeling and the effect on edge width. See DOI: 10.1039/c6nr08770a

We began by scrolling a Si/Cr (35/10 nm) bilayer nanostructure (Fig. 1) with a special "X" pattern (see ESI† and ref. 2). The Si layer was epitaxially grown by ultrahigh vacuum chemical vapor deposition on Si (001) at 550 °C followed by the deposition of a 10 nm thick amorphous Cr layer by e-gun evaporation. E-beam lithography, reactive ion etching, and wet etching were applied to form the rolled-up Si/Cr structures on Si (001). The energetically favorable scrolling directions of strained film on Si (001) substrate lie in <100>. Thus, the coiling directions of all the "fingers" lie in <100> and the coiled 3D structure can vary due to the presence of two possible perpendicular <100> directions, [100] and [010] on a Si (001) substrate. It was observed that the initial "X" shape, due to the misfit strain could form either a closed claw along the (100) direction (Fig. 1a) or an open claw perpendicular to the long sides (Fig. 1b). Each "finger" can snap to the other stable state independently, so intermediate stable states can also exist where the claw is partially closed (Fig. 1c). When the initial orientation of the micro-claw changes, its multistability also changes. A gutter-like structure (Fig. 1d) was observed when the micro-claw was rotated 45° so the "fingers" laid on the <110> directions. A nanorobotic manipulator installed inside a microscope was used to trigger the transition between two stable states. We provide a movie (see ESI†) to show that the global shape of the micro-claw can be changed from an open to a closed state. Our previous experiments showed that such a process is reproducible in practice and reversible in theory, although the reverse process is not easily achieved experimentally because of the size.[2] Similar multistability has been observed in natural and engineered systems.[15–17]

We first explained such phenomenon and demonstrated same configuration using table-top experiments.[18,19] We hypothesize that bistable bilayer structure can form at the nanoscale based on a principle similar to that at the macroscale, although the details of the driving force might be different, such as the edge effect studied in the micro-claws. We duplicated the phenomenon with a macroscopic table-top experiment using a measuring tape and induced equivalent stress conditions, which yielded similar "open" and "closed" bistability (see ESI†).

Despite identifying the mechanism at macroscopic scale, the role of the edge effect on bistability still remains to be explored at the nanoscale. Noticeably, the "fingers" in the open and closed configurations have curvatures with opposite sign. In the closed state, the longitudinal axis of the "fingers" is curved upwards around [100] and [010], whereas in the open state the transverse axis of the "fingers" curves down. A bistable sheet that is locally saddle-shaped can globally bend along either principal curvature, but not both at once. An early analytical model attributed the bistability to geometric nonlinear effects and negative intrinsic Gauss curvature.[20] Forming a bistable structure relies on introducing residual edge stresses. Using tensor analysis, Armon *et al.* explained how the bistability of a thin bilayer strip results from a combination of the stretching and the bending effect.[21] Several theoretical studies have provided a good understanding of the role of residual stresses and geometric nonlinearities on plate and shell bistability.[18,22] Recent numerical studies have also considered a similar combination of energies in helical ribbon multistability.[23] Overall, it is the nonlinear coupling between bending and stretching that drives the resulting stable configurations.[21]

In a strained Si/Cr micro-claw, the biaxial strain in the Cr layer serves as the primary driving force for scrolling, residual edge stresses in the Si layer due to the etching process play an important mechanical role in inducing bistability.[13] This edge stress is resulted from the fact that in the wet etching process the Si layer is 10–20 nm shorter than the Cr layer (this difference in width is hereafter referred to the underetching width).[9] As a result, the edge effect, or the edge stress, leads to an additional uniaxial stress which drives bistability, and is probably also responsible for the anomalous coiling.

We built on a previously developed theoretical framework and present analyses here on the role of the edge effect on the bistability of the bilayer structure.[22] According to our study, the bistability is governed by two dimensionless parameters (ζ and β) involving the driving force (*i.e.*, the surface stress f), material properties (E), and geometric parameters (width W and thickness h). In the following analyses and simulations, only one triangular "finger" was studied since each "finger" can snap independently. The plate (inset of the Fig. 2) is subjected to a biaxial surface stress f_1 on the top layer and an uniaxial surface stress f_e on the bottom layer as the edge effect. It should be noted that in our model the plate is assumed to be a single-layer sheet subjected to an effective surface stress.[22] We obtained the total energy of the system Π (see ESI†) at equilibrium and normalized the result to find the bifurcation threshold as a function of the principal curvatures (K_1, K_2), Young's modulus (E), layer thickness (h), and stress conditions (f_1 and f_e).

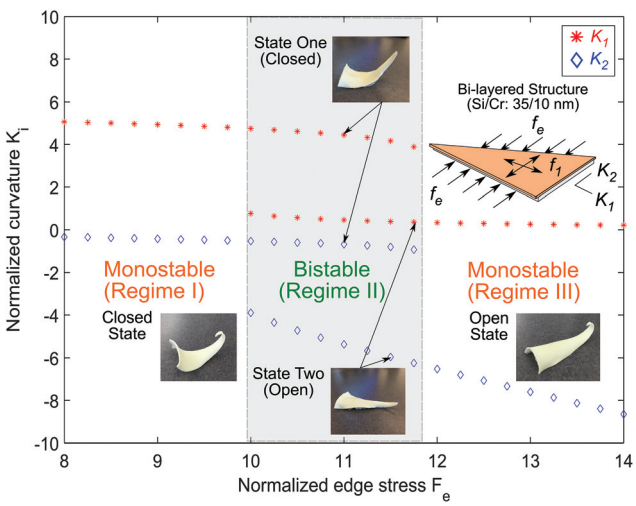

Fig. 2 Theoretical predicted morphological transition between monostable and bistable states when on the magnitude of the uniaxial edge stress f_e (edge effect) changes. Insets: stable states in each regime demonstrated by table-top experiments using elastic rubber sheets.

Fig. 2 shows the predicted phase diagram for edge effect $F_e = 6(1 - \nu^2)f_e/f_1$ *versus* normalized principal curvature $K_i = k_i EH^2/f_1$ (i = 1, 2). As normalized edge stress increases, the "finger" transitions from monostable to bistable and back again. Regime I has positive K_1 and nearly-zero K_2, so the strip will form a shape similar to the closed state of the micro-claw in Fig. 1a. In regime II, there is a solution group for each of the two stable states. As the edge effect increases into regime III, the strip will have a solution with a large K_2 and small K_1 and will look like the open state of the micro-claw in Fig. 1b.

We further validated the above prediction by performing a simple table-top experiment using rubber elastic sheets with the same geometrical parameters. Pre-stretched sheets are bonded to reinforced acrylic tape. The top layer is subjected to a biaxial strain (1.5%) and the magnitude of the strain in the bottom layer is varied from 2% to 4% to 6%. These insets of Fig. 2 showed that only one stable state was observed in regime I (open, small edge effect) and in regime III (closed, large edge effect), while regime II has both open and closed stable states, thus confirm that the edge effect drives bistability.

Many researchers have used continuum modeling[13,14,24–26] and atomic modeling[27–29] to study scrolling in multilayer nanostructures. Multiscale modeling approach is also available to combine both nanoscale atomic behaviors and macroscopic deformation.[30] A comprehensive summary of modeling nanostructures can be found in a recent review.[31] In this work, we applied the continuum modeling approach to capture the response behavior using the commercial (FEM) tool ABAQUS.[32] We run two simulation sets to further confirm the role of edge effect on bistability. The underetching width was fixed in first set while we studied the effect of underetching width on multiple micro-claws in the second set. The presence of the edge stress was equivalently modelled as having an effective edge strain in our simulations. Material properties, boundary condition and mesh strategy can be found in ESI.†

In the first set, two scenarios were tested for a plate that was subjected to a biaxial strain (1.5%) on the top layer and a uniaxial strain perpendicular to the edges on both sides. Fig. 3 shows the strain energy profile of the two scenarios (*i.e.*, with a small strain, 1%, and with a large strain, 5%, on the edge). As shown in Fig. 3, the modeling procedure includes four steps: (1) application of biaxial prestrain at t = 0; (2) application of edge strain at t = 1; (3) application of micro-manipulation force at t = 2; and (4) removal of micro-manipulation force at t = 3. Their corresponding deformed shapes and von Mises stresses are given as insets in Fig. 3. At t = 1, some amount of the strain energy has been released from the system after the Cr detached from the substrate, and the plate is in the closed configuration. After the edge strain is applied, both the low and high edge-effect plates stay in the closed state but the one with high edge-effect accumulated more strain energy compared to the one with low-edge effect. At t = 2, an external load is applied to both the low and high edge-effect plates, which trigger the open configuration. Finally, at t = 3 the "finger" with the small edge effect (blue dot line) snaps back to the closed configuration, but the "finger" with the large edge effect (red dash line) stays

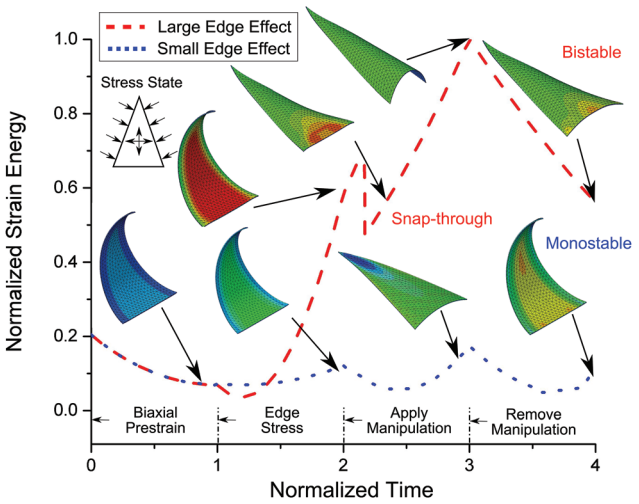

Fig. 3 Simulated snap-through of the "finger" under two magnitude of edge strain.

open. From the strain energy profile, we observe a significant drop soon after the manipulation force is applied to the high edge-effect "finger", which is indicative of snap-through buckling. The principal curvature diameter (d = 8.1 μm) generated through the simulation is consistent with the experimental data (d = 7.6 μm), and validate our theoretical prediction that the edge effect is the main driver of bistability.

In the second set, we ran multiple simulations with different combinations of misfit strain ratio ($|f_e/f_1|$) and underetching width ratio (W_e/W^*) to demonstrate the transition from monostability to bistability. It should be noted that the triangular part has a varying width along the longitudinal axis, and thus we use a mean width W^* calculated from an equivalent rectangular shape with same area. In this case, W^* is equal to 2000 nm. Fig. 4 shows a phase diagram

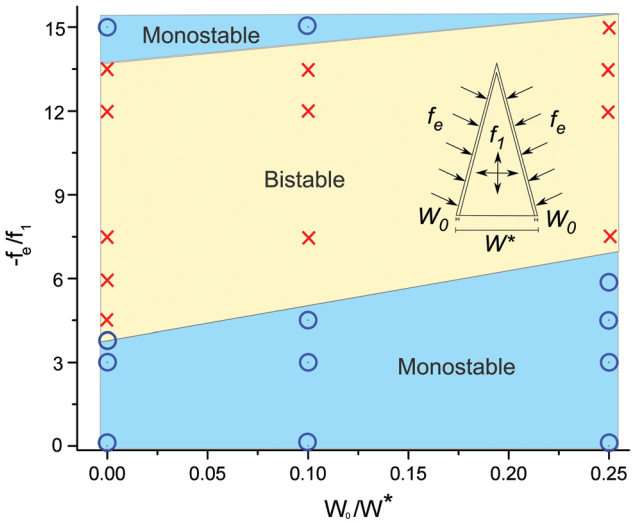

Fig. 4 The phase diagram of the Si/Cr micro-claw under the variation on misfit strain and the underetching width.

obtained from the numerical simulations. The vertical axis is the misfit strain ratio and the horizontal axis is the underetching width ratio. The first column is the results from a Si/Cr micro-claw with a very small underetching width (W_e/W = 0.01 or 20 nm), similar to the width from the experiments in Fig. 1. As expected, the "finger" shifts from monostable to bistable as the edge effect (vertical axis) increases. It is also consistent with the theoretical prediction that the structure will return to monostability if the edge effect is over the threshold value of $|f_e/f_1|$ = 14 as shown in Fig. 2. Within the bistable regime, the micro-claw also has a preferred first stable state, meaning whether it forms a closed or an open shape after detaching from the substrate. If $|f_e/f_1|$ is high (nearer to the top of the monostability region), the "finger" will form the closed shape, and *vice versa* if $|f_e/f_1|$ is low. Notably, as the underetching width ratio increases, the misfit strain ratio for the initial transition from a monostable state to a bistable state also increases (Fig. 4). As a result, the boundary that separates the regimes has a positive slope. It is due to the decrease of the total area of the bottom layer, which requires a greater contribution from the edge stress to overcome the stretching energy of the top layer and make the whole bilayer structure to snap through. We proved this observation using the theoretical model and obtained consistent results (see details in ESI†). Thus, we concluded that with the increase on the underetching width at the bottom layer, the transition from monostability to bistability is delayed.

Conclusions

This work illuminates, for the first time, the role of edge stress on the bistability of a microscale strained heterostructure with a nanometer-size thickness through a combined experimental, analytical, and numerical approach. We showed that a Si/Cr micro-claw transitions from monostable to bistable and back again as the magnitude of the edge effect is increased. If the edge effect can be controlled, bistability can be induced and programmed in other similar multilayer nanostructures such as nanobelts and nano-spirals. The mechanical self-assembly of strain-engineered flexible layers has broad applications in film-on-substrate electronics, NEMS/MEMS, and opto-electronics.[33] The addition of multistability will significantly enlarge the dimensionality and scope of its applications including nano- and micro-robotics, energy harvesting and drug delivery.

Acknowledgements

N. H. acknowledges Dr Likun Tan for her suggestions on the modeling. Z. C. acknowledges the support from the startup grant from the Thayer School of Engineering and the Society in Science – Branco Weiss fellowship, administered by ETH Zürich. L. Z. acknowledges the Early Career Scheme (ECS) grant with Project No. CUHK439113 from the Research Grants Council (RGC) of Hong Kong SAR. J. Z. acknowledges the NIH Director's Transformative Research Award (R01HL137157).

Notes and references

1 L. X. Dong, L. Zhang, D. J. Bell, D. Grützmacher and B. J. Nelson, *J. Phys.: Conf. Ser.*, 2007, **61**, 257.
2 L. Zhang, L. Dong, D. J. Bell, B. J. Nelson and D. A. Gruetzmacher, *IEEE International Conference on Nano/Micro Engineered and Molecular Systems*, 2006, DOI: 10.1109/NEMS.2006.334712.
3 L. Zhang, L. Dong and B. J. Nelson, *Appl. Phys. Lett.*, 2008, **92**, 243102.
4 X. Y. Kong and Z. L. Wang, *Nano Lett.*, 2003, **3**, 1625–1631.
5 D. J. Bell, T. E. Bauert, L. Zhang, L. X. Dong, Y. Sun, D. Grützmacher and B. J. Nelson, *Nanotechnology*, 2007, **18**, 055304.
6 G. Hwang, C. Dockendorf, D. Bell, L. Dong, H. Hashimoto, D. Poulikakos and B. Nelson, *Int. J. Optomechatroni.*, 2008, **2**, 88–103.
7 J. J. Abbott, M. Cosentino Lagomarsino, L. Zhang, L. Dong and B. J. Nelson, *Int. J. Rob. Res.*, 2009, **28**(11), 1434–1447.
8 S. V. Golod, V. Y. Prinz, P. Wägli, L. Zhang, O. Kirfel, E. Deckhardt, F. Glaus, C. David and D. Grützmacher, *Appl. Phys. Lett.*, 2004, **84**, 3391–3393.
9 L. Zhang, L. Dong, D. J. Bell, B. J. Nelson, C. Schönenberger and D. Grützmacher, *Microelectron. Eng.*, 2006, **83**, 1237–1240.
10 I. S. Chun, A. Challa, B. Derickson, K. J. Hsia and X. Li, *Nano Lett.*, 2010, **10**, 3927–3932.
11 L. Zhang, E. Deckhardt, A. Weber, C. Schönenberger and D. Grützmacher, *Nanotechnology*, 2005, **16**, 655.
12 L. Dai and L. Zhang, *Nanoscale*, 2013, **5**, 971–976.
13 L. Zhang, E. Ruh, D. Grützmacher, L. X. Dong, D. J. Bell, B. J. Nelson and C. Schönenberger, *Nano Lett.*, 2006, **6**, 1311–1317.
14 S. Kim, W. Kim, H. Chung and M. Cho, *RSC Adv.*, 2015, **5**, 96387–96391.
15 A. Pirrera, X. Lachenal, S. Daynes, P. M. Weaver and I. V. Chenchiah, *J. Mech. Phys. Solids*, 2013, **61**, 2087–2107.
16 Q. Guo, E. Dai, X. Han, S. Xie, E. Chao and Z. Chen, *J. R. Soc., Interface*, 2015, **12**, 20150598.
17 Z. Tian, L. Zhang, Y. Fang, B. Xu, S. Tang, N. Hu, Z. An, Z. Chen and Y. Mei, *Adv. Mater.*, 2017, DOI: 10.1002/adma.201604572.
18 Z. Chen, C. Majidi, D. J. Srolovitz and M. Haataja, *Appl. Phys. Lett.*, 2011, **98**, 011906.
19 Q. Guo, A. K. Mehta, M. A. Grover, W. Chen, D. G. Lynn and Z. Chen, *Appl. Phys. Lett.*, 2014, **104**, 211901.
20 E. Kebadze, S. D. Guest and S. Pellegrino, *Int. J. Solids Struct.*, 2004, **41**, 2801–2820.
21 S. Armon, E. Efrati, R. Kupferman and E. Sharon, *Science*, 2011, **333**, 1726–1730.
22 Z. Chen, Q. Guo, C. Majidi, W. Chen, D. J. Srolovitz and M. P. Haataja, *Phys. Rev. Lett.*, 2012, **109**, 114302.
23 Z. Chen, *Arch. Appl. Mech.*, 2014, **85**, 331–338.

24 L. Zhang, D. Xu, L. Dong and B. J. Nelson, *Microelectron. Eng.*, 2009, **86**, 824–827.
25 Z. Chen, *Nanoscale*, 2014, **6**, 9443–9447.
26 V. B. Shenoy, C. D. Reddy and Y.-W. Zhang, *ACS Nano*, 2010, **4**, 4840–4844.
27 D.-Y. Kim and S.-Y. Han, *J. Mech. Sci. Technol.*, 2015, **29**, 2111–2120.
28 Y. Nishidate and G. P. Nikishkov, *J. Appl. Phys.*, 2007, **102**, 083501.
29 Y. Nishidate and G. P. Nikishkov, *e-J. Surf. Sci. Nanotechnol.*, 2008, **6**, 301–306.
30 L. Tan, *Adv. Mater.*, 2016, **6**, 1–9.
31 K. F. Wang, B. L. Wang and T. Kitamura, *Acta Mech. Sin.*, 2015, **32**, 83–100.
32 Dassault Systèmes, *ABAQUS, User Manual Version 6.14*, 2015.
33 Z. Chen, G. Huang, I. Trase, X. Han and Y. Mei, *Phys. Rev. Appl.*, 2016, **5**, 017001.